Valley splitting in finite barrier quantum wells

Timothy B. Boykin
Department of Electrical and Computer Engineering, The University of Alabama in Huntsville, Huntsville, Alabama 35899, USA

Neerav Kharche
Network for Computational Nanotechnology, School of Electrical and Computer Engineering, Purdue University, West Lafayette, Indiana 47907, USA

Gerhard Klimeck
Network for Computational Nanotechnology, School of Electrical and Computer Engineering, Purdue University, West Lafayette, Indiana 47907, USA
and Jet Propulsion Laboratory, California Institute of Technology, 4800 Oak Grove Road, MS 169-315, Pasadena, California 91109, USA

(Received 19 October 2007; revised manuscript received 14 May 2008; published 23 June 2008)

The valley splitting (VS) in a silicon quantum well is calculated as a function of barrier height with both the multiband $sp^3d^5s^*$ model and a simple two-band model. Both models show a strong dependence of the VS on barrier height. For example, in both models some quantum wells exhibit a sharp minimum in the valley-splitting amplitude as the barrier height is changed. From the simple two-band model we obtain analytic approximations for the phases of the bulk states involved in the valley-split doublet, and from these we show that such sharp minima correspond to parity changes in the ground state as the barrier height is increased. The two-band analytic results show a complicated dependence of the valley splitting on barrier height, with the phases essentially being determined by a competition among effective quantum wells of differing length. These analytic results help explain the VS in realistic structures where different finite barrier heights are possible depending on the confining heterojunctions used.

DOI: 10.1103/PhysRevB.77.245320 PACS number(s): 73.21.Fg, 73.61.Cw, 73.43.Cd

I. INTRODUCTION

The electronic structure of conduction-band bound states in silicon quantum wells is particularly rich due to the properties of the bulk conduction-band minimum. In bulk, the *X*-valleys are sixfold degenerate, with minima occurring somewhat in from the Brillouin-zone faces. Strain can be applied along [001] to lift the sixfold degeneracy so that the degenerate valleys of interest are those lying along *z*. Because the minima lie completely within the Brillouin zone, there are four propagating states (with *z* wave vectors $\pm k_1, \pm k_2$ near the minima at $\pm k_{\min}$) at each energy within the valleys. In the simplest approximation, the quantum well bound states are linear combinations of all four propagating states, and as a result, the bound states occur in doublets. The splitting between the states comprising the lowest doublet is referred to as the valley splitting.

Most experimental[1] studies of this valley splitting in flatband silicon quantum wells are at finite magnetic field. Theoretical studies of infinite wells at zero magnetic field have used the two-valley effective-mass model[2] and tight-binding approaches.[3–6] The influence of electric fields on the valley splitting has also been investigated with two-valley effective mass,[7] simple tight-binding,[8] and $sp^3d^5s^*$ tight-binding approaches.[9] Theoretical investigations of the effect of finite barriers include numerical studies using the two-valley effective-mass,[7] pseudopotential,[10] and tight-binding approaches.[11,12] In contrast, there are relatively few zero magnetic-field experiments[13] and to our knowledge, none addresses the effect of barrier height on valley splitting for fixed well length.

Simple tight-binding models[3,4,8] have proven particularly useful for studying infinite-barrier flatband and V-shaped quantum wells, since these models permit analytic approximations which clarify much of the essential physics of valley splitting without any of the additional arbitrary fitting parameters found in the two-valley effective-mass approach.[2,7,14] In agreement with the much more complete $sp^3d^5s^*$ model, the simple tight-binding model demonstrates that the coupling of the four bulk states to yield two split bound states[3,4] produces the most striking features of the valley splitting in flatband quantum wells: its oscillation as a function of the quantum well length and the length dependence of the ground-state parity. These features have been predicted earlier[6] but have only recently been explained in detail.[3,4] The simple tight-binding model thus links the essential physics of valley splitting to more complete, but difficult to interpret, multiband calculations.

Finite barrier, flatband quantum wells exhibit similar valley-splitting behavior (oscillating valley splitting and parity of the ground state) to infinite-barrier quantum wells, but there are differing oscillation amplitudes and phase shifts in the valley splitting as a function of quantum well width.[4] The tight-binding investigations of finite barrier quantum wells to date have been numerical, while for the two-valley effective-mass model Ref. 7 presents analytic approximations. The overall similarity of finite and infinite-barrier systems is, however, insufficient for understanding some important properties of finite barrier systems. Tight-binding[12] and pseudopotential[10] calculations have shown significant changes in the valley splitting as a function of barrier height not seen in effective-mass[7] calculations. The purely numeri-

cal nature of the more complete models[10,12] obscures the reasons for this very different predicted behavior. A simple tight-binding approach, together with numerical, multiband results can clarify the reasons for this discrepancy and lead to a better understanding of the effect of barrier height.

Here we employ both a simple two-band tight-binding model[3,4,8] and the multiband $sp^3d^5s^*$ model[3,4,12,15] to study the valley splitting in flat, finite-barrier silicon quantum wells. In order to isolate the effect of the barrier height (as opposed to alloying and roughness in the barriers) we employ pure materials for the barriers. Our calculations show that the valley splitting can change significantly as a function of barrier height. In certain cases, notches in the valley splitting occur; the simple model shows that these correspond to parity flips of the ground state. Using the simple tight-binding model, we obtain approximate analytic expressions for the phase change in a finite barrier well as opposed to an infinite-barrier well. These expressions show that the valley splitting versus barrier height is a delicate interplay of phase shifts for different effective well lengths. This picture helps clarify some aspects of valley splitting in alloy barrier quantum wells because it shows that it is incorrect to think of the valley splitting an average of the valley splitting for different barriers. Instead one should think of the valley splitting as being governed by a weighted average of the *phases* appropriate to different infinite barriers.

II. METHOD

A. Bulk eigenstates

To model a Si quantum well grown along [001], we employ a one-dimensional tight-binding model consisting of a chain of identical atoms along the z direction, with one p_z orbital per atom.[3,4,8] The atomic separation is $a/2$, and interactions up to second-near-neighbor are included. As discussed in Refs. 3 and 4, one may view this model as either a two-band model, with two atoms per unit cell, length a, or a single-band model, with one atom per unit cell, length $a/2$. (The one-band model is in fact just a zone-unfolded two-band model, as expected.) The one-band description has the advantage of being mathematically much more tractable. However, because each unit cell of a flatband [001]-oriented Si quantum well consists of two atomic planes (one "anion" and one "cation" plane), one must parameterize the simple model so that the two-band version correctly mimics the lowest two conduction bands of Si. In our calculations we work in terms of the one-band phase, $\varphi = k^{(1)}a/2$, where $k^{(1)}$ is the one-band wave vector (different from the two-band wave vector, due to zone folding). The two-band model is parameterized so that minimum of its lower conduction band mimics that of Si in terms of position and longitudinal effective mass, and the resulting parameters are used in the mathematically simpler one-band version. Although we shall refer to the simple model as "two-band" since it is that version which is parameterized to mimic Si, from here on we work exclusively with the one-band formulation.

The wave function is written as

$$|\Psi\rangle = \sum_n C_n |z;n\rangle, \tag{1}$$

where the ket $|z;n\rangle$ is a p_z orbital on the atom indexed n and the C_n are expansion coeffieients which include the normalization; the orbitals are orthonormal. The Schrodinger equation in the tight-binding treatment appears as an infinite set of coupled equations. Within a bulklike region (all atoms of the same type and no applied fields) these equations take the form

$$u_\alpha C_{n-2} + v_\alpha C_{n-1} + (\varepsilon_\alpha - E)C_n + v_\alpha C_{n+1} + u_\alpha C_{n+2} = 0, \tag{2}$$

where $\alpha \in \{w,b\}$ denotes either the well (w) or the barrier (b) material. Both barriers will be taken to be semi-infinite and made of the same material. The onsite parameters are the ε_α, nearest-neighbor-coupling parameters are the v_α, and the second-near-neighbor-coupling parameters are the u_α. In order to keep the analytic treatment tractable, we assume that the same neighbor-coupling parameters apply to both materials, and that only the onsite parameters differ by a conduction-band offset W:

$$u_w = u_b = u, \quad v_w = v_b = v, \tag{3}$$

$$\varepsilon_w = \varepsilon, \quad \varepsilon_b = \varepsilon_w + W = \varepsilon + W. \tag{4}$$

The propagating state dispersion is found by substituting into Eq. (2) $C_n = \exp(in\varphi)$, $\varphi \in \mathrm{Re}$, where φ is the single-band phase introduced above. As shown in Ref. 4, the result is

$$E_\alpha(\varphi) = \varepsilon_\alpha + 2v\cos(\varphi) + 2u\cos(2\varphi). \tag{5}$$

Also from Ref. 4, the conduction-band minimum phase $\varphi_{\min}$ and energy satisfy

$$\cos(\varphi_{\min}) = -\frac{v}{4u}; \quad E_\alpha^{\min} = E_\alpha(\varphi_{\min}) = \varepsilon_\alpha - \frac{v^2}{4u} - 2u. \tag{6}$$

To reproduce the lowest conduction band of Si, we take the values from Ref. 4: $\varepsilon = 3.0$ eV, $v = 0.682640$ eV, and $u = 0.611705$ eV.

To find the evanescent (growing/decaying) states we require that in Eq. (2) the expansion coefficients be powers of a propagation factor, $\lambda : C_n = C_0\lambda^n$, then cancel out a common factor of $uC_0\lambda^{n-2}$ from Eq. (2) because $u \neq 0$, to obtain a quartic equation in λ. Since the minima occur somewhat inward from their respective Brillouin-zone faces, general properties of complex bands[16] indicate that the propagation factors λ ought to occur as a quartet: $\{\lambda, \lambda^*, 1/\lambda, 1/\lambda^*\}$. Some algebra shows that the four solutions of this quartic equation are

$$\lambda = e^{\pm\theta \pm i\beta}, \quad \theta,\beta \in \mathrm{Re}\,., \tag{7}$$

where to satisfy Eq. (2) with $C_n = C_0\lambda^n$, the $\beta - \theta$ relationship and the energy are

$$\cosh(\theta)\cos(\beta) = -\frac{v}{4u} = \cos(\varphi_{\min}), \tag{8}$$

$$E_\alpha^{\mathrm{evanesc}}(\theta,\beta) = \varepsilon_\alpha - 4u\cosh^2(\theta) - 4u\cos^2(\beta) + 2u. \tag{9}$$

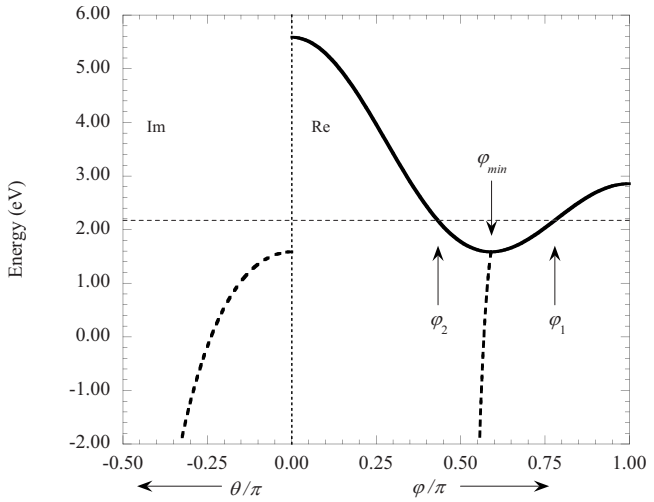

FIG. 1. Real and complex bands of the one-band version of the two-band model used in the text. Real bands and parts of bands are plotted on the positive axis and imaginary parts of bands are plotted on the negative axis. The heavy solid line on the positive axis is the conduction band. The conduction-band minimum phase is denoted by $\varphi_{\min}$ and two degenerate bulk states contributing to one state of a valley-split pair are indicated by the phases φ_1, φ_2. The heavy dashed lines show the real and imaginary band pair beginning just below the conduction-band minimum. (In the text the phase of the real part of this pair is denoted β, with φ reserved for the conduction band itself.)

In Fig. 1 we graph the real and complex bands of the one-band version of the two-band model. Note in particular that the evanescent state phase β lies between the valley minimum phase $\varphi_{\min}$ and $\pi/2$, varying little over a fairly wide energy range. In Sec. II C, this slow variation will allow us to make some useful simplifying approximations.

Because the well and barrier states have the same energy, $E_w(\varphi) = E_b^{\text{evanesc}}(\theta, \beta)$, the phases of the valley-split states in the quantum well are related to the decay/propagation constants in the barriers. For states involved in valley splitting, $E_w^{\min} < E < E_b^{\min} = E_w^{\min} + W$, and requiring equality of the two energy functions yields

$$\cos^2(\beta) = \frac{1}{2}[\mathcal{B} - \sqrt{\mathcal{B}^2 - 4\cos^2(\varphi_{\min})}], \quad \cos(\beta) = -\sqrt{\cos^2(\beta)}, \tag{10}$$

$$\mathcal{B} = \left[1 + \frac{W}{4u} + \cos^2(\varphi_{\min})\right] - [\cos(\varphi) - \cos(\varphi_{\min})]^2, \tag{11}$$

where the second part of Eq. (10) follows from Eq. (8) which shows that $\cos(\beta) \leq 0$. Likewise, the phases in the well of the two valley-split states are related. (In Fig. 1, φ_1, φ_2 label two such bulk states.) Requiring in Eq. (5) that $E_w(\varphi_1) = E_w(\varphi_2)$ and noting that $\cos(\varphi_1) \neq \cos(\varphi_2)$, one finds

$$\begin{aligned} \cos(\varphi_1) + \cos(\varphi_2) &= -\frac{v}{2u} \\ &= 2\cos(\varphi_{\min}) \\ &\Rightarrow \cos(\bar{\varphi})\cos(\delta) = \cos(\varphi_{\min}), \end{aligned} \tag{12}$$

where the last equation is written in terms of an average phase and average phase difference, $\bar{\varphi} = (\varphi_1 + \varphi_2)/2$, $\delta = (\varphi_1 - \varphi_2)/2$.

B. Quantum well eigenstates: exact transcendental equations

The quantum well consists of $(2N+1)$ atoms, indexed $n = -N, \ldots, N$. The barriers are identical and semi-infinite; the left extending for $n \leq -(N+1)$, the right for $n \geq (N+1)$. Because the Hamiltonian is symmetric about $n = 0$, the coefficients C_n in Eq. (1) can be taken as even or odd. (Note that because the basis states are p_z orbitals, the wave-function parity is opposite that of the coefficients.) The even (e) and odd (o) coefficients are thus

$$C_n^{(e)} = \begin{cases} [b_1^{(e)}\cos[\beta^{(e)}(n+N+1)] + b_2^{(e)}\sin[\beta^{(e)}(N+1+n)]]\exp[\theta^{(e)}(N+1+n)], & n \leq -(N+1) \\ a_1^{(e)}\cos(n\varphi_1^{(e)}) + a_2^{(e)}\cos(n\varphi_2^{(e)}), & -N \leq n \leq N \\ [b_1^{(e)}\cos[\beta^{(e)}(N+1-n)] + b_2^{(e)}\sin[\beta^{(e)}(N+1-n)]]\exp[\theta^{(e)}(N+1-n)], & n \geq (N+1) \end{cases}, \tag{13}$$

$$C_n^{(o)} = \begin{cases} -[b_1^{(o)}\cos[\beta^{(o)}(n+N+1)] + b_2^{(o)}\sin[\beta^{(o)}(N+1+n)]]\exp[\theta^{(o)}(N+1+n)], & n \leq -(N+1) \\ a_1^{(o)}\sin(n\varphi_1^{(o)}) + a_2^{(o)}\sin(n\varphi_2^{(o)}), & -N \leq n \leq N \\ [b_1^{(o)}\cos[\beta^{(o)}(N+1-n)] + b_2^{(o)}\sin[\beta^{(o)}(N+1-n)]]\exp[\theta^{(o)}(N+1-n)], & n \geq (N+1) \end{cases}. \tag{14}$$

The transcendental equations which determine the phases involved in the valley-split states are found by solving the four equations at either barrier/well interface; we solve those at the right barrier interface. These four equations are of the form of Eq. (2),

$$uC_{n-2}^{(\alpha)} + vC_{n-1}^{(\alpha)} + [\varepsilon_n - E]C_n^{(\alpha)} + vC_{n+1}^{(\alpha)} + uC_{n+2}^{(\alpha)} = 0, \tag{15}$$

where $n = (N-1), \ldots, (N+2)$ and $\varepsilon_n = \varepsilon$, $n \leq N$; $\varepsilon_n = \varepsilon + W$, $n \geq (N+1)$. The process is considerably simplified by recognizing that each of the interface equations is easily converted

to a purely bulk equation (equal to zero) plus an additional term, which is therefore also equal to zero. At the right interface, introduce the notation for the coefficients:

$$\chi_n^{(e)} = a_1^{(e)} \cos(n\varphi_1^{(e)}) + a_2^{(e)} \cos(n\varphi_2^{(e)}), \tag{16}$$

$$\chi_n^{(o)} = a_1^{(o)} \sin(n\varphi_1^{(o)}) + a_2^{(o)} \sin(n\varphi_2^{(o)}), \tag{17}$$

$$\eta_n^{(\alpha)} = \{b_1^{(\alpha)} \cos[(N+1-n)\beta^{(\alpha)}] + b_2^{(\alpha)} \sin[(N+1-n)\beta^{(\alpha)}]\}\exp[(N+1-n)\theta^{(\alpha)}]. \tag{18}$$

Note that the $\chi_n^{(\alpha)}$ are solutions of the well bulk equations while the $\eta_n^{(\alpha)}$ are solutions of the barrier bulk equations.

One first solves the $n=(N+2)$ interface equation, Eq. (15), adding and subtracting $u\eta_N^{(\alpha)}$ in the notation of Eqs. (16)–(18) for the $C_n^{(\alpha)}$. Part of the result is a bulk equation (equal to zero) so that the remaining term $u[\chi_N^{(\alpha)} - \eta_N^{(\alpha)}]$ is likewise zero. This result is used in the $n=(N+1)$ interface equation after adding and subtracting the term $v\eta_{N-1}^{(\alpha)} + u\eta_N^{(\alpha)}$. The process is repeated for the other interface equations, and because $u, v \neq 0$ the resulting four equations take the same form:

$$\chi_n^{(\alpha)} - \eta_n^{(\alpha)} = 0, \quad n = (N-1), \ldots, (N+2). \tag{19}$$

The four equations (19) therefore constitute a system of homogeneous equations for the even (e) and odd (o) coefficients, the $a_j^{(\alpha)}$ and $b_j^{(\alpha)}$.

Rearranging each homogeneous system into matrix form and requiring the determinants of the respective matrices to vanish finally result in the transcendental equations satisfied by the even- and odd-coefficient states. After some trigonometric simplifications and dividing out a factor $\sin(\beta^{(\alpha)}) > 0$, one finds for both states

$$\sum_{m=-1}^{3} c_m^{(\alpha)} \exp[(m-3)\theta^{(\alpha)}] = 0, \tag{20}$$

$$c_3^{(\alpha)} = f_\alpha^{(N+1,1)}, \tag{21}$$

$$c_2^{(\alpha)} = -2\cos(\beta^{(\alpha)}) f_\alpha^{(N,2)}, \tag{22}$$

$$c_1^{(\alpha)} = f_\alpha^{(N-1,3)} + [4\cos^2(\beta^{(\alpha)}) - 1] f_\alpha^{(N,1)}, \tag{23}$$

$$c_0^{(\alpha)} = -2\cos(\beta^{(\alpha)}) f_\alpha^{(N-1,2)}, \tag{24}$$

$$c_{-1}^{(\alpha)} = f_\alpha^{(N-1,1)}. \tag{25}$$

where

$$f_e^{(n,m)} = \cos[(n+m)\varphi_1^{(e)}]\cos(n\varphi_2^{(e)}) - \cos(n\varphi_1^{(e)})\cos[(n+m)\varphi_2^{(e)}], \tag{26}$$

$$f_o^{(n,m)} = \sin[(n+m)\varphi_1^{(o)}]\sin(n\varphi_2^{(o)}) - \sin(n\varphi_1^{(o)})\sin[(n+m)\varphi_2^{(o)}]. \tag{27}$$

Observe that as $W \to \infty$, $\theta^{(\alpha)} \to \infty \Rightarrow \exp[-q\theta^{(\alpha)}] \to 0$, and $q > 0$, so that Eq. (20) becomes the appropriate infinite-barrier transcendental equation,[4] as expected. Using trigonometric identities, the $f_\alpha^{(n,m)}$ may be rewritten compactly in terms of the $\bar{\varphi}^{(\alpha)}$ and $\delta^{(\alpha)}$ as defined following Eq. (12):

$$f_\alpha^{(n,m)} = -\{\sin[(2n+m)\delta^{(\alpha)}]\sin(m\bar{\varphi}^{(\alpha)}) + P_\alpha \sin[(2n+m)\bar{\varphi}^{(\alpha)}]\sin(m\delta^{(\alpha)})\}, \tag{28}$$

where

$$P_e = +1, \quad P_o = -1. \tag{29}$$

The form of the $f_\alpha^{(n,m)}$ in Eq. (28) is well suited for finding the approximate phases of the bulk states comprising the valley-split pair.

C. Quantum well eigenstates: approximate solution

Approximate solutions of the transcendental equations are most easily found for quantum wells which are at least of moderate length. As in Ref. 4, the objective is to use these transcendental equations to find approximations for the $\delta^{(\alpha)}$, from which the approximate valley splitting may be calculated. Thus, in approximating the $f_\alpha^{(n,m)}$ we are interested in cases $|m| \ll n$, where $m=1,2,3$. Furthermore, for the lowest-lying valley-split pair,[4] $\delta^{(\alpha)} \approx \pi/(2n+m)$, so that the angle $|\pi - (2n+m)\delta^{(\alpha)}| \ll 1$. Hence, we may rewrite the factors in Eq. (28) in terms of small angles and make appropriate small-angle approximations:

$$\sin[(2n+m)\delta^{(\alpha)}] = \sin[\pi - (2n+m)\delta^{(\alpha)}] \approx \pi - (2n+m)\delta^{(\alpha)}, \tag{30}$$

$$\sin(m\delta^{(\alpha)}) \approx m\delta^{(\alpha)}. \tag{31}$$

Doing so, the $f_\alpha^{(n,m)}$ are approximately

$$f_\alpha^{(n,m)} \approx -P_\alpha m\delta^{(\alpha)} \sin[(2n+m)\bar{\varphi}^{(\alpha)}] - \pi \sin(m\bar{\varphi}^{(\alpha)}) + (2n+m)\delta^{(\alpha)} \sin(m\bar{\varphi}^{(\alpha)}). \tag{32}$$

Using Eq. (32) along with Eqs. (20)–(27), results in a lowest-order solution of the respective transcendental equations for the average phase differences $\delta^{(\alpha)}$:

$$\delta^{(\alpha)} \approx \frac{\pi \mathcal{N}^{(\alpha)}}{\mathcal{D}_1^{(\alpha)} - P_\alpha \mathcal{D}_2^{(\alpha)}}, \tag{33}$$

$$\mathcal{N}^{(\alpha)} = \sin(\bar{\varphi}^{(\alpha)}) - 2\exp[-\theta^{(\alpha)}]\cos(\beta^{(\alpha)})\sin(2\bar{\varphi}^{(\alpha)}) + \exp[-2\theta^{(\alpha)}]\{\sin(3\bar{\varphi}^{(\alpha)}) + \sin(\bar{\varphi}^{(\alpha)})[4\cos^2(\beta^{(\alpha)}) - 1]\} - 2\exp[-3\theta^{(\alpha)}]\cos(\beta^{(\alpha)})\sin(2\bar{\varphi}^{(\alpha)}) + \exp[-4\theta^{(\alpha)}]\sin(\bar{\varphi}^{(\alpha)}), \tag{34}$$

$$\mathcal{D}_1^{(\alpha)} = (2N+3)\sin(\bar{\varphi}^{(\alpha)}) - 2(2N+2)\exp[-\theta^{(\alpha)}]\cos(\beta^{(\alpha)})\sin(2\bar{\varphi}^{(\alpha)}) + \exp[-2\theta^{(\alpha)}](2N+1)$$
$$\times\{\sin(3\bar{\varphi}^{(\alpha)}) + \sin(\bar{\varphi}^{(\alpha)})[4\cos^2(\beta^{(\alpha)}) - 1]\} - 4N\exp[-3\theta^{(\alpha)}]\cos(\beta^{(\alpha)})\sin(2\bar{\varphi}^{(\alpha)}) + (2N-1)\exp[-4\theta^{(\alpha)}]\sin(\bar{\varphi}^{(\alpha)}), \tag{35}$$

$$\mathcal{D}_2^{(\alpha)} = \sin[(2N+3)\bar{\varphi}^{(\alpha)}] - 4\exp[-\theta^{(\alpha)}]\cos(\beta^{(\alpha)})\sin[(2N+2)\bar{\varphi}^{(\alpha)}] + \exp[-2\theta^{(\alpha)}]\sin[(2N+1)\bar{\varphi}^{(\alpha)}]\{3 + [4\cos^2(\beta^{(\alpha)}) - 1]\}$$
$$- 4\exp[-3\theta^{(\alpha)}]\cos(\beta^{(\alpha)})\sin(2N\bar{\varphi}^{(\alpha)}) + \exp[-4\theta^{(\alpha)}]\sin[(2N-1)\bar{\varphi}^{(\alpha)}]. \tag{36}$$

These equations are still fairly complicated, so further approximations are helpful. Physical intuition suggests that less accurate, but more easily computed, approximations can be tolerated in the barriers (not in the well, of course). Thus, we use somewhat crude but easily computed formulas for the barrier regions. Because the even- and odd-coefficient valley-split states are so close in energy it is physically reasonable to ignore the differences between the $\beta^{(\alpha)}$ and $\theta^{(\alpha)}$. We therefore drop the distinguishing superscripts. Furthermore, using results from Ref. 4, to lowest order in $\delta^{(\alpha)}$,

$$\cos(\varphi_1^{(\alpha)}) - \cos(\varphi_{\min}) \approx -\delta^{(\alpha)}\sin(\varphi_{\min}), \tag{37}$$

so that using Eq. (37) in Eqs. (10) and (11), the lowest-order approximation yields

$$\cos(\beta) \approx \frac{\cos(\varphi_{\min})}{\sqrt{1 + W/(4u) + \cos^2(\varphi_{\min})}}. \tag{38}$$

Equation (38), together with Eq. (8) results in a quadratic equation for the exponential factors, whose solution is

$$e^{-\theta} \approx \sqrt{1 + W/(4u) + \cos^2(\varphi_{\min})} - \sqrt{W/(4u) + \cos^2(\varphi_{\min})}. \tag{39}$$

From Ref. 4, we take there the lowest-order approximation $\bar{\varphi}^{(\alpha)} \approx \varphi_{\min}$ in $\sin(\bar{\varphi}^{(\alpha)})$ and $\sin[(2N+m)\bar{\varphi}^{(\alpha)}]$, $m=-1,\ldots,3$ as well. Introducing these approximations and Eqs. (37) and (38) in Eqs. (33)–(36), together with the general expression for the approximate valley splitting in terms of the $\delta^{(\alpha)}$,[4]

$$\Delta E = E(\varphi_1^{(o)}) - E(\varphi_1^{(e)}) \approx 4u\sin^2(\varphi_{\min})[\delta^{(o)} - \delta^{(e)}][\delta^{(o)} + \delta^{(e)}] \tag{40}$$

gives the approximate expression for the valley splitting in finite barrier systems. Note that the presence of the exponential factors, together with the rapidly oscillating terms $\sin[(2N+m)\varphi_{\min}]$ means that the valley splitting is a delicate interplay between phases for different effective quantum well lengths weighted by decay constants. As will be shown below, this interplay can effectively shift the valley-splitting curve by a fraction of a cell length, thereby greatly changing the splitting.

III. RESULTS

Figure 2 graphs the valley splitting versus number of atoms $S=2N+1$ as calculated with four different models: the simple two-band model presented in Sec. II with either finite (0.4 eV) or infinite barriers, and the nearest-neighbor $sp^3d^5s^*$ model with 1.525 eV barriers, with and without spin-orbit coupling. The barriers are simulated with carbon parameters taken from Ref. 15, with a variable conduction-band offset (here 1.525 eV); the silicon parameters are from Refs. 17 and 18. The two-band results come from numerical solution of the even- and odd-coefficient versions of the exact finite-barrier transcendental equation, Eq. (20), for the $\varphi_1^{(\alpha)}$. The valley splitting is then calculated as $|\Delta E| = |E(\varphi_1^{(o)}) - E(\varphi_1^{(e)})|$, where $E(\varphi)$ is defined in Eq. (5). In the broadest sense, the curves are similar in shape and period, but with differing amplitudes and phase shifts. In other calculations with different confinement methods, we have observed a sensitivity of the valley-splitting amplitude. Similar sensitivity to the barrier height has been noted in other recent work.[19] This sensitivity implies a strong dependence on the evanescent states responsible for the confinement, and because these evanescent states are necessarily different in the simple and multiband tight-binding models, the difference in valley-splitting amplitude between them is not surprising. Qualitatively, though, the two models are in agreement, and in both cases it is abundantly clear that for a fixed quantum well size

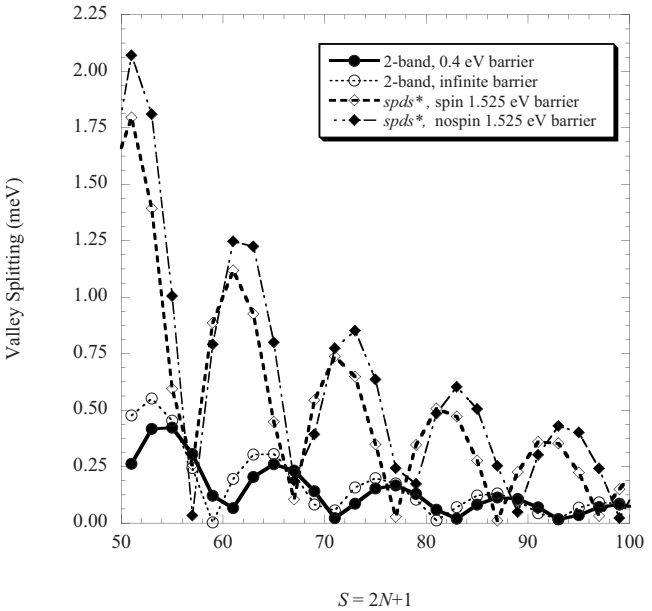

FIG. 2. Valley splitting versus number of atoms (two-band model) or atomic planes ($sp^3d^5s^*$ model) for different barrier heights, and in the case of the $sp^3d^5s^*$ model, both with and without spin-orbit interaction included in the calculation.

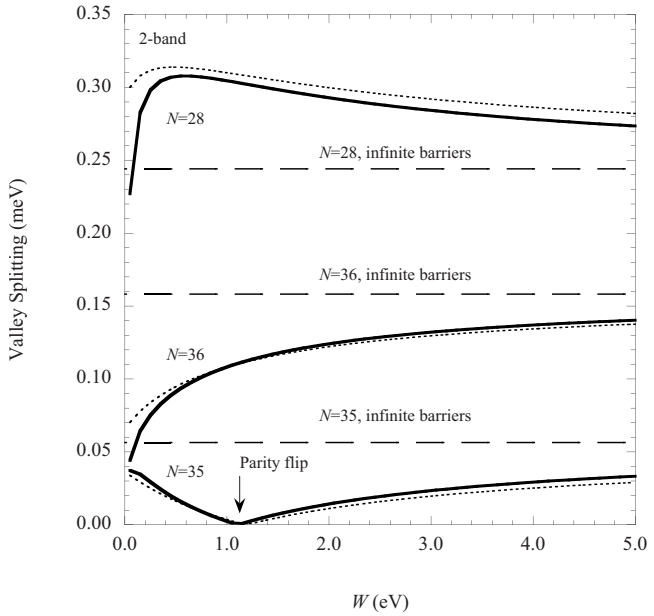

FIG. 3. Valley splitting versus barrier height for different quantum well lengths in the two-band model. The number of atoms in each well is $S=(2N+1)$. Solid lines are the exact valley splitting, dotted lines the approximate valley splitting discussed in the text. Dashed horizontal lines indicate the infinite-barrier valley splitting for each of the wells. Note the sharp minimum for the $N=35$ well, where a parity flip occurs.

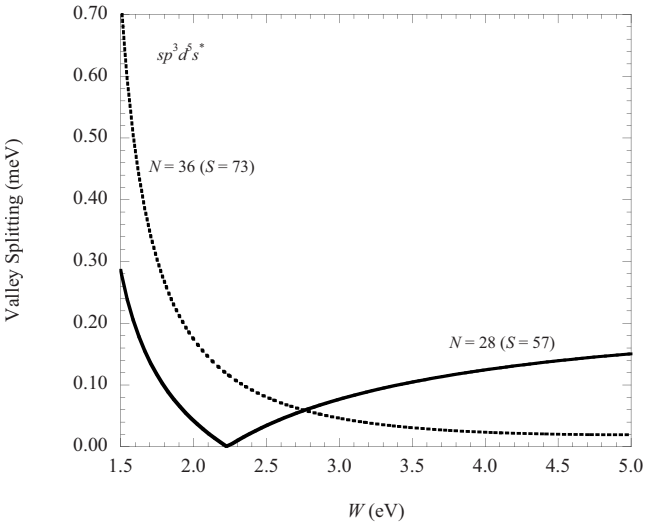

FIG. 4. Valley splitting in the $sp^3d^5s^*$ model for two different quantum well lengths versus barrier height. Note the sharp minimum like that seen in the two-band results of Fig. 3.

S, the valley splitting can change significantly with the barrier height. This behavior is in contrast to the two-valley effective-mass model[7] where the valley splitting is independent of barrier height.

Close examination of the both the two-band and multiband results reveals that a variety of behavior is possible as the barrier height is changed for a fixed quantum well size. Figure 3 for the two band model graphs the exact, finite barrier valley splitting (solid lines) and the approximate splitting (dotted lines), along with the exact infinite-barrier splitting (horizontal dashed lines) for three different quantum wells. The approximate valley splitting is $|\Delta E|$ from Eq. (40) with approximations [Eqs. (37)–(39)] and $\bar{\varphi}^{(\alpha)} \approx \varphi_{\min}$ in Eqs. (33)–(36) as discussed in Sec. II C. Observe that the valley splitting can simply rise to its infinite-barrier value ($N=36$), exceed it, then fall back toward it ($N=28$), or reach a sharp minimum, then rise back toward the infinite-barrier value ($N=35$). The sharp minimum in this last case occurs because at that point the parity of the ground state changes, as indicated on the graph. Similar parity flips can occur in V-shaped quantum wells as the field strength (slope of the V) is changed.[8]

The multiband nearest-neighbor $sp^3d^5s^*$ results (Fig. 4) show similar behavior, with one exception: the strong tendency toward a fairly large valley splitting at low barrier heights. As discussed above, this type of behavior is seen in some quantum wells in the simple two-band model, but not others. Just like in the simple model, however, sharp minima can occur in the valley splitting of the multiband model ($N=28$). While the two models do not agree on the exact details of the valley-splitting behavior, it is important to keep in mind that in order to make the two-band model tractable, only the conduction-band offset between the two materials was changed. In the multiband model, the barrier, and the interface parameters are different from those of the well. In addition, the evanescent states of the two-band model are much simpler than are those of the $sp^3d^5s^*$ model. The two-band model can nevertheless provide qualitative explanations of the multiband results.

The analytic results of Sec. II help to clarify the valley-splitting dependence on quantum well size. For quantum wells that are not too short, we may take $(2N+m) \approx (2N+3)$, $m=-1,\ldots,2$, so that $\mathcal{D}_1 \approx (2N+3)\mathcal{N}$, where we drop superscripts since in the lowest-order approximation we take $\bar{\varphi}^{(\alpha)} \approx \varphi_{\min}$ and, as in Eqs. (49)–(51), $\beta^{(\alpha)} \approx \beta$, $\theta^{(\alpha)} \approx \theta$. Equation (33) for the $\delta^{(\alpha)}$ then reads:

$$\delta^{(\alpha)} \approx \frac{\pi}{(2N+3)} + P_\alpha \frac{\pi}{(2N+3)^2} \frac{\mathcal{D}_2}{\mathcal{N}}, \tag{41}$$

so that the approximate valley splitting is, from Eq. (40),

$$\Delta E \approx -16u \sin^2(\varphi_{\min}) \left[\frac{\pi^2}{(2N+3)^3} \right] \left(\frac{\mathcal{D}_2}{\mathcal{N}} \right). \tag{42}$$

Note that $\mathcal{D}_2$ is a sum of fast-oscillating terms for different effective quantum well lengths, weighted by the appropriate barrier decay and phase factors. Which of these effective quantum wells dominates depends on where each of the $\sin[(2N+m)\varphi_{\min}]$ terms is its cycle, as well as the barrier height, which determines the decay factors via Eq. (39).

The presence and nature of the competition between different effective quantum wells in the simple tight-binding model account for the difference between our results and those of Ref. 7. In the two-valley effective-mass model,[7] the barrier height is proportional to the valley coupling parameter and therefore there is no barrier height dependence of the valley splitting. Part of the insensitivity to barrier height is due to the fact that the results of Ref. 7 are to lowest order

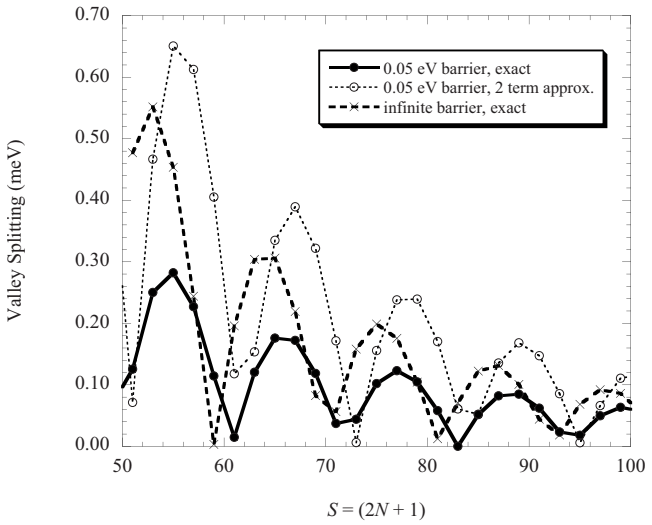

FIG. 5. Valley splitting versus number of atoms $S=(2N+1)$ in the two-band model for both 0.05 eV barriers and infinite barriers. For the 0.05 eV barrier case the splitting is calculated exactly and with the two-term approximation discussed in the text. Note the enhanced oscillation amplitude when only the two slowest-decaying terms are retained.

only, and when higher order corrections are included, a barrier height dependence appears. Yet, even with these corrections, parity flips have not been observed. The way in which the valley coupling parameter in Ref. 7 is determined is the probable cause for the remaining differences. The barrier height dependence of this parameter was determined by fitting to a simple tight-binding numerical calculation of valley splitting versus quantum well length at fixed barrier height. Thus, the valley coupling parameter in Ref. 7 necessarily involves averaging over quantum well lengths. Seen in the light of Eqs. (33)–(42), this averaging tends to upset the phase relationships in the $\mathcal{D}_2$ term above. Hence, the fine structure of the valley splitting versus barrier height (for fixed well length) tends to be washed out.[20]

Due to the multiband nature of the $sp^3d^5s^*$ model it is not strictly correct to speak of a difference term $(\delta^{(o)}-\delta^{(e)})$ for it, but this concept remains useful because four bulk states dominate the wave function in the quantum well. In this light, observe that as the $sp^3d^5s^*$ model is a nearest-neighbor model, its effective difference term should be a competition among fewer effective quantum well lengths. To see if this observation might point toward factors behind the enhanced valley splitting at low barrier heights, we can use the analytic results of the two-band model. Here we make a very crude approximation in the expressions for the $\mathcal{D}_2$ and $\mathcal{N}$, retaining only the two slowest-decaying terms in $\exp(-m\theta)$, $m=0,1$. In Fig. 5 we graph the valley splitting versus $S=(2N+1)$ for barrier height $W=0.05$ eV as calculated both exactly and with the two-term approximation, along with the infinite-barrier valley splitting as a reference. Interestingly, the admittedly crude two-term approximation shows a tendency toward larger amplitude oscillations; for low barriers this increase is partly due to a smaller $\mathcal{N}$. While these results do not completely explain the tendency of the multiband model toward increased valley splitting at low barrier heights, they do suggest that the shorter-range interaction of this model limits the number of effective quantum wells competing to determine the valley splitting.

Finally, we emphasize that the two-band analytic results show clearly that the valley splitting cannot be seen as a sum of valley splittings for different quantum well lengths, simply because the valley splitting is defined as an absolute value. Instead, the different effective quantum wells contribute the phases and especially the critical phase difference $(\delta^{(o)}-\delta^{(e)})\sim\mathcal{D}_2/\mathcal{N}$. Note that although the fast-oscillating terms appear only in the numerator $\mathcal{D}_2$, the denominator $\mathcal{N}$ still changes with the barrier height. That the result can be rather complex and highly dependent on where the fast-oscillating terms are in their respective cycles is clear from Figs. 3 and 4, especially as regards minima resulting from a parity-flip.

IV. CONCLUSIONS

We have shown that changing the barrier height for a fixed quantum well length can greatly affect the valley splitting, using both a simple two-band model and the multiband $sp^3d^5s^*$ model; these effects are not seen in the two-valley effective-mass[7] approach. For the two-band model we have obtained analytic approximations for the phases of the bulk states involved in the valley-split pair which show that in the finite-barrier case there is effectively a competition among different effective-length quantum wells to determine the valley splitting. The outcome of this competition depends on where the various fast-oscillating terms are in their respective cycles together with the barrier height, which determines the multiplicative decay factor for the effective quantum wells. There is of course no decay in the terms arising from the actual quantum well. These results show that sharp minima in the valley splitting are due to parity flips, where the ground state changes parity as the barrier height is increased. Similar minima are seen in the multiband results. Finally, we have used the analytic results to examine the effect fewer competing quantum wells on the valley splitting by dropping terms which decay more quickly. Retaining only the constant and slowest-decaying term tends to enhance the amplitude of the valley-splitting oscillations with quantum well length, suggesting that the fewer effective quantum wells competing in the nearest-neighbor $sp^3d^5s^*$ model may be a contributing factor to the enhanced valley splitting at low barrier heights.

ACKNOWLEDGMENTS

We thank M. Friesen for discussions. This work was supported by Semiconductor Research Corporation and the Army Research Office. The work described in this publication was carried out in part at the Jet Propulsion Laboratory, California Institute of Technology under a contract with the National Aeronautics and Space Administration, and Jet Propulsion Laboratory. Calculations were performed on nanohub.org resources provided by the Network for Computational Nanotechnology, funded by the National Science Foundation.

[1] See, for example, A. B. Fowler, F. F. Fang, W. E. Howard, and P. J. Stiles, Phys. Rev. Lett. **16**, 901 (1966); F. F. Fang and P. J. Stiles, Phys. Rev. **174**, 823 (1968); H. Koehler, M. Roos, and G. Landwehr, Solid State Commun. **27**, 955 (1978); R. J. Nicholas, K. von Klitzing, and T. Englert, *ibid.* **34**, 51 (1980); J. Wakabayashi, S. Kimura, Y. Koike, and S. Kawaji, Surf. Sci. **170**, 359 (1986); V. M. Pudalov, A. Punnoose, G. Brunthaler, A. Prinz, and G. Bauer, arXiv:cond-mat/0104347 (unpublished); R. B. Dunford, R. Newbury, F. F. Fang, R. G. Clark, R. P. Starrett, J. O. Chu, K. E. Ismail, and B. S. Meyerson, Solid State Commun. **96**, 57 (1995); S. J. Koester, K. Ismail, and J. O. Cho, Semicond. Sci. Technol. **12**, 348 (1996); P. Weitz, R. J. Haug, K. von. Klitzing, and F. Schäffler, Surf. Sci. **361-362**, 542 (1996); D. Monroe, Y. H. Xie, E. A. Fitzgerald, and P. J. Silverman, Phys. Rev. B **46**, 7935 (1992); S. F. Nelson, K. Ismail, J. J. Nocera, F. F. Fang, E. E. Mendez, J. O. Chu, and B. S. Meyerson, Appl. Phys. Lett. **61**, 64 (1992); G. Stöger, G. Brunthaler, G. Bauer, K. Ismail, B. S. Meyerson, J. Lutz, and F. Kuchar, Phys. Rev. B **49**, 10417 (1994).

[2] F. J. Ohkawa, Solid State Commun. **26**, 69 (1978).

[3] Timothy B. Boykin, Gerhard Klimeck, M. A. Eriksson, Mark Friesen, S. N. Coppersmith, Paul von Allmen, Fabiano Oyafuso, and Senugwon Lee, Appl. Phys. Lett. **84**, 115 (2004).

[4] T. B. Boykin, G. Klimeck, M. Friesen, S. N. Coppersmith, P. von Allmen, F. Oyafuso, and S. Lee, Phys. Rev. B **70**, 165325 (2004).

[5] R. D. Graft, D. J. Lohrmann, G. P. Parravicini, and L. Resca, Phys. Rev. B **36**, 4782 (1987).

[6] J.-C. Chiang, Jpn. J. Appl. Phys., Part 2 **33**, L294 (1994).

[7] M. Friesen, S. Chutia, C. Tahan, and S. N. Coppersmith, Phys. Rev. B **75**, 115318 (2007).

[8] T. B. Boykin, G. Klimeck, P. von Allmen, S. Lee, and F. Oyafuso, J. Appl. Phys. **97**, 113702 (2005).

[9] M. Virgilio and G. Grosso, Phys. Rev. B **75**, 235428 (2007).

[10] A. Valavanis, Z. I. Ikonic, and R. W. Kelsall, Phys. Rev. B **75**, 205332 (2007).

[11] M. O. Nestoklon, L. E. Golub, and E. L. Ivchenko, Phys. Rev. B **73**, 235334 (2006).

[12] N. Kharche, M. Prada, T. B. Boykin, and G. Klimeck, Appl. Phys. Lett. **90**, 092109 (2007).

[13] K. Takashina, Y. Ono, A. Fujiwara, Y. Takahashi, and Y. Hirayama, Phys. Rev. Lett. **96**, 236801 (2006).

[14] M. Friesen, C. Tahan, R. Joynt, and M. A. Eriksson, Phys. Rev. Lett. **92**, 037901 (2004).

[15] J.-M. Jancu, R. Scholz, F. Beltram, and F. Bassani, Phys. Rev. B **57**, 6493 (1998).

[16] T. B. Boykin, Phys. Rev. B **54**, 8107 (1996); **54**, 7670 (1996).

[17] T. B. Boykin, G. Klimeck, and F. Oyafuso, Phys. Rev. B **69**, 115201 (2004).

[18] T. B. Boykin, N. Kharche, and G. Klimeck, Phys. Rev. B **76**, 035310 (2007).

[19] M. O. Nestoklon, E. L. Ivchenko, J.-M. Jancu, and P. Voisin, Phys. Rev. B **77**, 155328 (2008).

[20] M. Friesen (private communication).